Numerical Simulation Study for Frequency Sharing Between Micro-Cellular Systems and Fixed Service Systems in Millimeter-Wave Bands

JOONGHEON KIM[1], LIANG XIAN[2], AND ALI S. SADRI[2]
[1]Chung-Ang University, Seoul 156-756, South Korea
[2]mmWave Standards and Advanced Technology Team, Intel Corporation, Santa Clara, CA 95054, USA

ABSTRACT This paper presents numerical simulation results to study the impact of the co-existence between a fixed service (FS) system and 5G small cell networks at 28-, 38-, and 60-GHz millimeter-wave (mmWave) frequency bands. For this paper, two scenarios are considered: aggregation of interference from small cells into an FS receiver from base stations (BSs) to their associated user equipment (UE) (downlink) and the aggregation of cellular interference at the FS receiver from UEs to their associated BSs (downlink). Moreover, mmWave-specific propagation characteristics and attenuation factors are considered for a more precise simulation study. The simulation results determine how much interference rejection is required to protect the operation of FS. In addition, currently available mmWave modular antenna array (MAA) architectures are introduced. Based on the information, additional mmWave frequency sharing study is performed using the realistic MAA radiation patterns. Last, we compare and analyze the performance differences between ITU standard models and MAA solutions.

INDEX TERMS Millimeter-wave, frequency sharing study, 28 GHz, 38 GHz, 60 GHz, 5G, modular antenna array.

I. INTRODUCTION

Among the various requirements for next-generation 5G cellular networks, achieving multi-gigabits-per-second (multi-Gbps) rates is one of the major requirements. In order to achieve the requirement, millimeter-wave (mmWave) wireless communication technologies have been mainly considered including those being studied for 28 GHz [3]–[8], 38/39GHz [9], [10], and 60 GHz [11], [12] frequency bands [13]–[21].

The use of mmWave, or near-mmWave frequency bands for 5G networks provides the opportunity to use ultra-wideband spectrum, increased channel capacity, and potential for spatial densification. All these benefits come at the expense of potentially greater system complexity especially in terms of radio frequency (RF) front-end and antenna design. However, the recent advancements in mmWave wireless systems and platform development have produced cost effective solutions that can be leveraged to overcome these challenges.

The other challenge in accessing mmWave and near-mmWave bands is the protection of incumbents. In this paper, we performed intensive numerical simulations to analyze interference between mmWave small cell systems and fixed service (FS) stations at 28 GHz, 38 GHz, and 60 GHz in the same or adjacent geographical areas. This study was performed to identify (i) how much potentially harmful interference will be injected into FS receiver station and (ii) how much interference should be mitigated to enable co-existence between small-cell networks and FS systems.

This type of numerical simulation study for calculating co-existence harmful interference in new frequency bands is essential for discussing in ITU meetings in order to verify that the candidate frequency bands are adequate for next generation wireless network design and deployment. This study is named *frequency sharing study* in wireless standard activities.

For this study, both downlink and uplink interference scenarios are considered, i.e., (i) aggregation of interference into an FS receiver antenna generated by every single wireless transmission from small cell base stations to their associated users (i.e., downlink interference); and (ii) aggregation of interference into an FS receiver antenna

generated by every single wireless transmissions from small cell users to their associated base stations (i.e., uplink interference). Using 28 GHz, 38 GHz and 60 GHz radio wave mmWave propagation characteristics and inter-ference calculation methods, actual amounts of required frequency rejection are calculated through Monte Carlo simulations.

Even though this paper considers 28 GHz, 38 GHz, and 60 GHz mmWave frequency bands as potential 5G frequency bands, the proposed sharing study methodologies are appli-cable for the other frequency bands when the required param-eters are provided. In 5G research, E-bands are also actively discussed. However, conducting frequency sharing study for E-bands is not doable at this moment because required param-eters (e.g., FS system parameters) are not fully provided yet [22].

Lastly, this paper considers existing 60 GHz modular antenna array (MAA) antenna radiation patterns. The MAA architecture is widely studied in wireless communication societies according to its benefits in terms of flexibility and effectiveness. We investigated our own 60 GHz mmWave MAA RF systems/hardware and the MAA parameters such as transmit/receive antenna gains and transmit powers are used for frequency sharing study. Therefore, quick introduction to MAA is included in this paper (see Section VI). Moreover, the frequency sharing study conducted again includes measured MAA radiation patterns together with ITU-standard radiation patterns. Finally, this paper shows the performance differ-ence depending on the antenna patterns (standard patterns vs. MAA antenna patterns) and explains where the difference comes from.

Our previous frequency sharing study results are presented and discussed in [1] and [2] and this paper differs from the results in many ways: (i) each result in [1] and [2] is only for one dedicated mmWave frequency band, i.e., [1] is for 39 GHz and [2] is for 60 GHz, whereas this paper considers three major 5G candidate frequencies; and (ii) the results in [1] and [2] are obtained from theoretical and standard radiation patterns whereas this paper additionally contains measured MAA antenna radiation patterns which include certain amounts of sidelobe/backlobe levels.

This kind of frequency sharing study is essential in order to use mmWave wireless technologies in cellular networks for determining weather newly deployed cellular systems can co-existence with pre-deployed FS systems or not. If the frequency sharing study results say that both systems may generate harmful interference to each other (from small cells to FS systems, and vice versa, then the cellular network engineers should implement additional functionalities for interference mitigation and suppression. On the other hand, the frequency sharing study results say that both systems will not generate harmful interference to each other, both cellular systems and FS systems can co-exist without any additional techniques for interference mitigation and suppres-sion. Therefore, this study is essential for cellular network deployments in any frequency bands; and also should be

conducted before deploying cellular network components in the frequency band.

The remainder of this paper is organized as follows: Section II presents reference network topology which is used for this frequency sharing study. Section III explains 28 GHz, 38 GHz and 60 GHz mmWave radio wave propagation models and characteristics. Section IV describes the details of frequency sharing study procedures in both downlink and uplink interference scenarios. Section V presents Monte Carlo simulation results and corresponding explanations. Section VI briefly introduces existing MAA RF hardware and platforms. Section VII presents the performance of the frequency sharing study with the existing MAA platforms and antenna patterns. Section VIII concludes this paper.

II. NETWORK MODEL FOR FREQUENCY SHARING STUDY
The small-cell network layout is as illustrated in Fig. 1 where 19 cells are arranged in a hexagonal pattern with each cell consisting of three sectors. In this paper, we assume that the cell radius is 100 m because of short-distance communication natures in mmWave wireless communications [23], [24]. A small cell BS is located at the center of each small cell and operates with a three-sector antenna. In addition, the average number of active UE in each sector at any given time is set to 3.
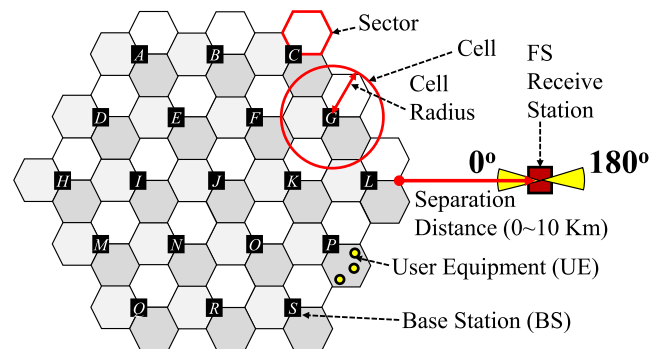

FIGURE 1. Network layout for the frequency sharing study between cellular systems and FS systems.

As shown in Fig. 1, an FS receive station is initially located at the right edge of the 19 small cells (so called *origin*), and the sharing study in terms of required frequency rejection performed through varying the separation distance from the origin from 0 up to 10 Km far away the origin. In addition to these parameter configurations, two different orientations are assumed for the FS receiver antenna, i.e., 0° and 180°. Notice that the two orientations show the lower and upper bounds of system performance in terms of interference injection.

III. mmWAVE PROPAGATION MODELS AND PARAMETERS
This section introduces mmWave specific propagation models and parameters. ITU-defined reference antenna radia-tion patterns are presented in Section III-A, mmWave specific path-loss models are in Section III-B, and mmWave specific attenuation factors are lastly presented in Section III-C.

A. REFERENCE ANTENNA RADIATION PATTERNS [25]

The ITU-recommended reference antenna radiation patterns for sharing studies from 400 MHz to about 70 GHz are presented in ITU Recommendation ITU-R F.1336-4 [25]. As proposed in [25] (and also summarized in [1] and [2]), the ITU-recommended reference antenna radiation patterns can be numerically plotted as shown in Fig. 2 when transmit antenna gains are 39.2 dBi in FS (refer to Fig. 2(a)), 24 dBi in BS (refer to Fig. 2(b)), and 15 dBi in UE (refer to Fig. 2(c)). Notice that detailed numerical formulations are presented in [1] and [2].

B. PATH-LOSS MODELS

Free-space basic transmission loss in a dB scale is given as a function of path length d_{Km} in a Km scale by ITU Recommendation ITU-R P.1411-8 [26]:

$$PL\left(f_c, d_{Km}\right) = 92.44 + 20\log_{10}\left(f_c\right) + n \cdot 10\log_{10}\left(d_{Km}\right) \tag{1}$$

where f_c stands for the carrier frequencies in a GHz scale and n is path-loss coefficient that is set to $n = 2.2$ for line-of-sight (LoS) propagation when $f_c \geq 10$ [26]. Even though non-line-of-sight (NLoS) propagation is also of interest, mmWave NLoS path-loss models for long-distance scenarios (from 1 Km to 50 Km) is not investigated yet to the best of our knowledge. In addition, ITU Recommendation ITU-R P.1411 [26] clearly states that mmWave signal coverage is considered only for free-space propagation because of the large diffraction losses experienced when obstacles cause the propagation path to become NLoS. Therefore, this paper only considers free-space propagation and the extension with NLoS path-loss will be investigated when the corresponding models are available.

C. mmWAVE SPECIFIC ATTENUATION FACTORS

As explained in [26], attenuation by atmospheric gases (which is also called oxygen attenuation) and by rain must be considered in mmWave radio wave propagation.

The oxygen attenuation behaviors depending on carrier frequencies are measured and presented in Fig. 3. As shown in Fig. 3 obtained from [27] (and also presented in [30] only for 60 GHz), the oxygen attenuation factors in 28 GHz, 38 GHz, and 60 GHz mmWave bands are about 0.11 dB/Km, 0.13 dB/Km, and 16 dB/Km, respectively.

The rain attenuation factors depends on the rain climatic zones those are segmented and measured by the ITU as presented in ITU Recommendation ITU-R PN.837-1 [29]. Reference [29, Table 1] presents the rain rates depending on the ITU-recommended segmented areas (from ITU Region **A** to ITU Region **Q**). In this paper, ITU Region **D** (which is for Northern California (CA), Oregon (OR), and Washington (WA)) and ITU Region **Q** (which is for the heaviest rain areas such as Middle Africa) are of our interests. Table 1 presents the rain rates of ITU regions **D** and **Q** (unit: mm/h); and their corresponding rate attenuation
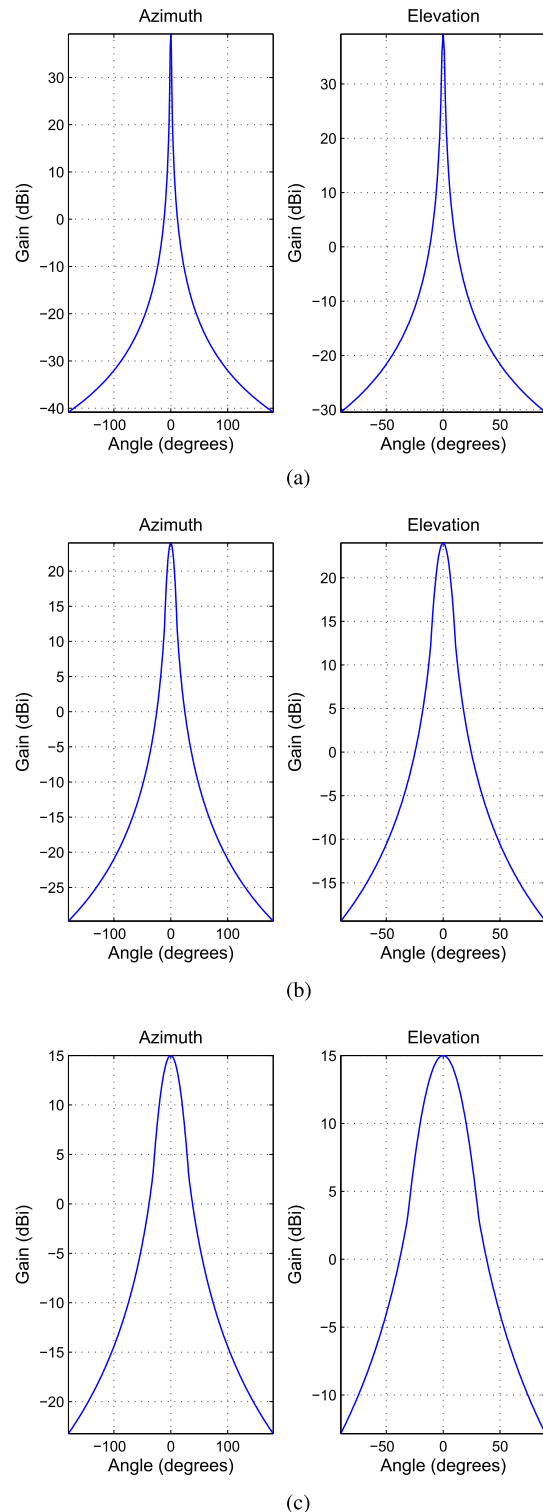

FIGURE 2. Reference antenna radiation patterns for the fixed and mobile services for use in sharing studies (ITU F.1336-4 [25]). (a) FS (Tx antenna again: 39.2 dBi, $\theta_{BW} = \varphi_{BW} \approx 1.93°$). (b) BS (Tx antenna gain: 24 dBi, $\theta_{BW} = \varphi_{BW} \approx 11.11°$). (c) UE (Tx antenna gain: 15 dBi, $\theta_{BW} = \varphi_{BW} \approx 31.31°$).

factors (unit: dB/Km) which depend on various outage probabilities (1.0% and 0.1%) based on [28] and Fig. 4. The Table 1 presents rain attenuation factors in various ITU
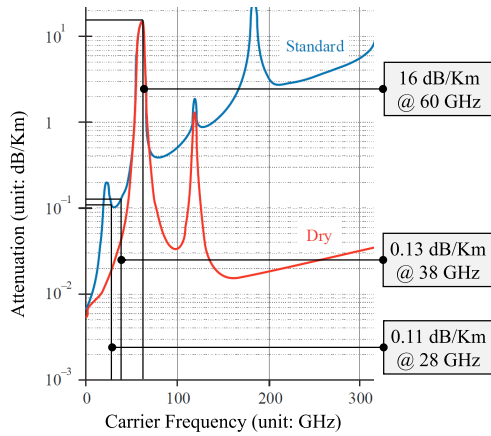
FIGURE 3. Attenuation by atmospheric gases, i.e., oxygen attenuation [27].

TABLE 1. Rain Rates (unit: mm/h, i.e., millimeter per hour) and their corresponding attenuation factors (unit: dB/Km, i.e., decibel per kilometer) at 28 GHz, 38 GHz, and 60 GHz mmWave bands depending on rain climatic zones (especially for ITU Regions D and Q) [29].

f_c	ITU Region	1% Outage	0.1% Outage
28 GHz	ITU Region D	2.1 mm/h	8 mm/h
	(Northern CA, OR, WA)	(0.25 dB/Km)	(1.4 dB/Km)
	ITU Region Q [Heavy rain]	24 mm/h	72 mm/h
	(Middle Africa, *et. al.*)	(4 dB/Km)	(12 dB/Km)
38 GHz	ITU Region D	2.1 mm/h	8 mm/h
	(Northern CA, OR, WA)	(0.6 dB/Km)	(2.0 dB/Km)
	ITU Region Q [Heavy rain]	24 mm/h	72 mm/h
	(Middle Africa, *et. al.*)	(6 dB/Km)	(17 dB/Km)
60 GHz	ITU Region D	2.1 mm/h	8 mm/h
	(Northern CA, OR, WA)	(1.2 dB/Km)	(3.5 dB/Km)
	ITU Region Q [Heavy rain]	24 mm/h	72 mm/h
	(Middle Africa, *et. al.*)	(9 dB/Km)	(25 dB/Km)

Regions **D** and **Q**, various outage probabilities (1.0% and 0.1%), and various mmWave frequency bands, i.e., 28 GHz, 38 GHz, and 60 GHz.

IV. COEXISTENCE FREQUENCY SHARING STUDY BETWEEN MICRO-CELLULAR SYSTEMS AND FIXED SERVICE SYSTEMS IN mmWAVE BANDS

This section includes the detailed procedures for frequency sharing study. The fundamental objective methodologies are presented in Section IV-A, and co-channel and adjacent channel interference calculation procedures are discussed in Section IV-B and Section IV-C, respectively.

A. OBJECTIVE AND METHODOLOGIES

The objective of this frequency sharing study is to numerically identify the amounts of *required frequency rejection* as a function of separation distance that would allow compatible operation of mmWave micro-cell systems and FS stations. For the study, two separated interference scenarios are considered, i.e., (i) downlink interference scenario and (ii) uplink interference scenario.

After calculating accumulated interferences in both downlink and uplink interference scenarios, the required frequency
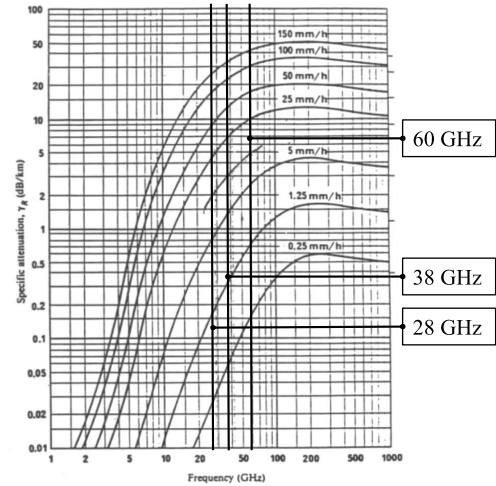

FIGURE 4. Attenuation by rain rates [28].

TABLE 2. Estimated 28 GHz and 38 GHz parameters from 60 GHz MAA platform parameters.

	28 GHz	38 GHz
Transmit antenna gain (unit: dBi)	18.0	20.1
Transmit power (unit: dBm)	11.4	14.0
Receive antenna gain (unit: dBi)	9.0	11.1

rejection needed to meet protection requirement at the FS receiver antenna (denoted as R) can be calculated as follows:

$$R = \mathcal{I}^* - \mathcal{N} - \gamma_{\text{requirement}} \qquad (2)$$

where $\mathcal{I}^*$ stands for the accumulated interference (for both co-channel and adjacent-channel interferences), $\mathcal{N}$ stands for the FS receive antenna noise power density, i.e.,

$$\mathcal{N} = N_{\text{FS}}^{\text{thermal}} + 10 \log_{10}\left(\frac{B_{\text{FS}}}{10^6}\right) + N_{\text{FS}}^{\text{F}} \qquad (3)$$

where $N_{\text{FS}}^{\text{thermal}}$ is a receiver thermal noise [22], B_{FS} is a channel bandwidth in an FS receiver, N_{FS}^{F} is a receiver noise figure [22], and $\gamma_{\text{requirement}}$ in (2) means the required interference-per-noise, i.e., I/N, for protection of FS (presented in Table 3). If $\mathcal{I}^* \leq \gamma_{\text{requirement}}$, we do not need to suppress or mitigate any interference injection because the co-existence between FS systems and small cell systems is possible without any interference rejection. On the other hand, i.e., $\mathcal{I}^* > \gamma_{\text{requirement}}$, we need to suppress $\left(\mathcal{I}^* - \gamma_{\text{requirement}}\right)$ amount of interferences for the co-existence between FS systems and micro-small cell systems.

All required parameters for FS, BS, and UE, are summarized in Table 3. In Table 3, antenna gain and transmit power parameters are measured with 60 GHz mmWave RF hardware and systems. However, we have to estimate the parameters in 28 GHz and 38 GHz because the system is now under development. Notice that the transmit antenna gain, receive antenna gain, and transmit power are measured as 24 dBi (TX-MAA8, i.e., transmitter with the MAA

TABLE 3. Parameters and models in various mmWave bands.

			28 GHz	38 GHz	60 GHz
FS Parameters	Rx antenna gain at FS k: $G_{FS,k}^{Rx}(0,0)$				39.2 dBi
	Height: h_{FS} [31]				30 m
	Channel bandwidth: B_{FS} [22]		60 MHz	56 MHz	50 MHz
	Rx noise figure: N_{FS}^{F} [22]		8 dB	6.3 dB	7 dB
	Thermal noise at Rx: $N_{FS}^{thermal}$ [22]		-136 dBm/Hz	-137.7 dBm/Hz	-137 dBm/Hz
	Required I/N for protection of FS: $\gamma_{requirement}$ [22]				-10 dB
BS Parameters	The number of deployed BSs				19
	The number of sectors in each BS cell				3
	Cell radius r				100 m
	Tx antenna gain at BS i: $G_{BS,i}^{Tx}(0,0)$		18.0 dBi (Table II)	20.1 dBi (Table II)	24 dBi
	Tx power at BS i: $P_{BS,i}$		11.4 dBm (Table II)	14.0 dBm (Table II)	19 dBm
	Height: h_{BS} [32]				6 m
	Channel bandwidth: B_{BS}		200 MHz	500 MHz [1]	2.16 GHz [24]
UE Parameters	The number of active UEs in each sector				3
	Tx antenna gain		9.0 dBi (Table II)	11.1 dBi (Table II)	15 dBi
	Maximum Tx power at UE j: $P_{UE,j}^{max}$		2.4 dBm	5 dBm	10 dBm
	minimum Tx power at UE j: $P_{UE,j}^{min}$		-47.6 dBm	-45 dBm	-40 dBm
	Height: h_{UE} [32]				1.5 m
	Channel bandwidth: B_{UE}		200 MHz	500 MHz [1]	2.16 GHz [24]
Propagation models	Reference antenna radiation pattern [25]		ITU Recommendation for Sharing Study [25]		
	Path-loss (free-space) [26], [33]		(1) where $n = 2.2$		
	Oxygen attenuation [27]		0.11 dB/Km	0.13 dB/Km	16 dB/Km
	Rain attenuation at ITU Region D (1.0% outage) [28], [29]		0.25 dB/Km	0.6 dB/Km	1.2 dB/Km
	Rain attenuation at ITU Region D (0.1% outage) [28], [29]		1.4 dB/Km	2.0 dB/Km	3.5 dB/Km
	Rain attenuation at ITU Region Q (1.0% outage) [28], [29]		4 dB/Km	6 dB/Km	9 dB/Km
	Rain attenuation at ITU Region Q (0.1% outage) [28], [29]		12 dB/Km	17 dB/Km	25 dB/Km

equipped with 8 modules), 15 dBi (RX-MAA1, i.e., receiver with the MAA equipped with 1 module), and 19 dBm in the 60 GHz links with TX-MAA8 and RX-MAA1. We suppose that the link budget at 28 GHz and 38 GHz bands should show equivalent performance to the link budget calculation results at 60 GHz in terms of RF hardware implementation complexity. The 60 GHz IEEE 802.11ad[1] baseband defines three different modulation schemes in its set of modulation and coding schemes (MCSes), i.e., BPSK (from MCS0 to MCS5), QPSK (from MCS6 to MCS9), and 16QAM (from MCS10 to MCS12). It means the modulation scheme changes in two points, i.e., (i) from MCS10 to MCS9 (i.e., from 16QAM to QPSK) and (ii) from MCS6 to MCS5 (i.e., from QPSK to BPSK). In this paper, we consider the first point, i.e., from MCS10 to MCS9, because mmWave systems are usually for small cell systems (i.e., short transmission range). Let this point be named *critical point*. Therefore, 28 GHz and 38 GHz link budget calculation results need to show that their MCS10 should change to MCS9 when the distance between transmitter and receiver is 159.4 m under the assumption that the three mmWave RF systems have equivalent hardware implementation complexity. As presented in

FIGURE 5. Link (between TX-MAA8 and RX-MAA1) budget calculation for 28 GHz, 38 GHz, and 60 GHz mmWave bands: the three systems achieve MCS10 in a same distance.

Fig. 5, we tunes and estimates the antenna gain and transmit power parameters in 28 GHz and 38 GHz for letting them have same critical points in 28 GHz, 38 GHz, and 60 GHz mmWave bands. Based on this estimation, the parameters for 28 GHz and 38 GHz platforms are obtained as shown in Table 2. Intel implemented 60 GHz IEEE 802.11ad RFIC and modem, few years ago. On top of the valuable experience, we are now conducting 28 GHz system implementation and also expect that the values in Table 2 are precisely realized.

[1]IEEE 802.11ad is the most successful standard among mmWave wireless standards and this is equivalent to Wireless Gigabit Alliance (WiGig) standard.
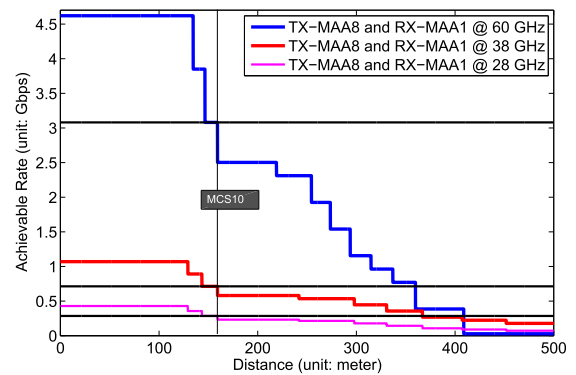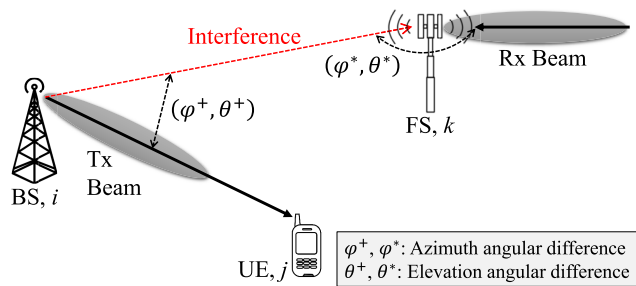
FIGURE 6. Illustration of downlink interference scenarios.

B. CO-CHANNEL INTERFERENCE CALCULATION

1) INDIVIDUAL DOWNLINK CO-CHANNEL INTERFERENCE CALCULATION

For calculating individual downlink interference $I_{(i,j)}^{\text{DL}}$, i.e., every single interference to an FS receive antenna generated by the transmission from micro-cellular BS i to its associated UE j,

$$I_{(i,j)}^{\text{DL}} = f_{\text{BW-scale}}\left(P_{\text{BS},i} + G_{\text{BS},i}^{\text{Tx}}\left(\varphi^+, \theta^+\right)\right) \\ - L\left(f_c, d_{(i,k)}\right) + G_{\text{FS},k}^{\text{Rx}}\left(\varphi^*, \theta^*\right) \quad (4)$$

is being calculated where $I_{(i,j)}^{\text{DL}}$ stands for the generated interference to the FS receive antenna of k due to the downlink transmission from micro-cellular BS i to its associated UE j, $G_{\text{BS},i}^{\text{Tx}}\left(\varphi^+, \theta^+\right)$ is the transmit antenna gain to the receive antenna of FS generated by the downlink transmission from micro-cellular BS i to its associated UEs; and the angular differences between the downlink transmission and interference directions in azimuth and elevation planes are denoted as φ^+ and θ^+ are illustrated in Fig. 6. For the angular difference computation, the heights of FS, BS, and UE are set to 30 m, 6 m, and 1.5 m, respectively.
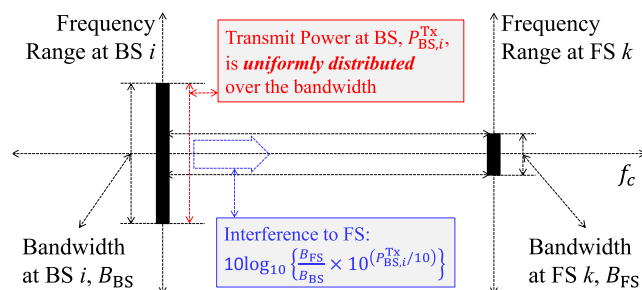

FIGURE 7. Received power calculation at an FS receive antenna k from micro-cellular BS i in a same frequency band.

As shown in Fig. 7, all transmit power from BS i is not fully affecting on an FS receiver antenna. Due to the fact that the bandwidths in BS and FS are not same, the received interference at an FS receive antenna is proportional to the bandwidth difference as shown in Fig. 7. Therefore, the received power at an FS receiver antenna k from micro-cellular BS i,

i.e., $f_{\text{BW-scale}}(x)$, can be calculated as follows:

$$f_{\text{BW-scale}}(x) = 10\log_{10}\left\{\frac{B_{\text{FS}}}{B_{\text{BS}}} \times 10^{\left(\frac{x}{10}\right)}\right\} \quad (5)$$

where B_{FS} stands for the channel bandwidth at an FS system and B_{BS} stands for the channel bandwidth at a micro-cellular BS (set to 200 MHz at a 28 GHz band, 500 MHz at a 38 GHz band, and 2.16 GHz at a 60 GHz band). Note that the channel bandwidth of BS is same as the one of UE such as in a time division duplexing (TDD) system.

In addition, $G_{\text{FS},k}^{\text{Rx}}\left(\varphi^*, \theta^*\right)$ in (4) is the antenna gain of an FS receive antenna generated by the downlink transmission from micro-cellular BS i to its associated UE and the corresponding angular differences in azimuth and elevation planes, i.e., φ^* and θ^*, can be calculated as illustrated in Fig. 6. For computing $G_{\text{BS},i}^{\text{Tx}}\left(\varphi^+, \theta^+\right)$ and $G_{\text{FS},k}^{\text{Rx}}\left(\varphi^*, \theta^*\right)$, the ITU-recommended reference antenna radiation patterns of BS and FS are required; and the details about the reference radiation patterns are explained in Section III-A. In (4), $L\left(f_c, d_{(i,k)}\right)$ stands for the mmWave wireless signal power loss (or attenuation) from micro-cellular BS i to FS receive antenna k. The loss can be obtained as follows:

$$L\left(f_c, d_{(i,k)}\right) = PL\left(f_c, d_{(i,k)}\right) + O\left(f_c, d_{(i,k)}\right) \\ + R\left(f_c, d_{(i,k)}\right) \quad (6)$$

where $PL\left(f_c, d_{(i,k)}\right)$, $O\left(f_c, d_{(i,k)}\right)$, and $R\left(f_c, d_{(i,k)}\right)$ stand for path-loss (calculating with (1)), attenuation due to oxygen absorption (0.11 dB/Km, 0.13 dB/Km, and 16 dB/Km at 28 GHz, 38 GHz, and 60 GHz), and rain attenuation (refer to Table 1) depending on distance and carrier frequency, respectively.

After calculating individual downlink interference with (4), overall accumulated interference (i.e., $\mathcal{I}$ in (2)) at an FS receiver antenna can be obtained by summing all calculated downlink interference values in a linear scale as follows:

$$\mathcal{I} = \sum_{\forall i \in S_{\text{BS}}} \sum_{\forall j \in S_{\text{UE},i}} I_{(i,j)}^{\text{DL}} \quad (7)$$

where S_{BS} is a set of micro-cellular BSs and $S_{\text{UE},i}$ is a set of the UEs that is associated with micro-cellular BS $i \in S_{\text{BS}}$.

2) INDIVIDUAL UPLINK CO-CHANNEL INTERFERENCE CALCULATION

For calculating individual uplink interference $I_{(j,i)}^{\text{UL}}$, i.e., individual interference to an FS receive antenna generated by the transmission from UE j to its associated micro-cell BS i,

$$I_{(j,i)}^{\text{UL}} = f_{\text{BW-scale}}\left(P_{\text{UE},j}^{\text{Tx}} + G_{\text{UE},j}^{\text{Tx}}\left(\varphi^+, \theta^+\right)\right) \\ - L\left(f_c, d_{(j,k)}\right) + G_{\text{FS},k}^{\text{Rx}}\left(\varphi^*, \theta^*\right) \quad (8)$$

is being calculated where $I_{(j,i)}^{\text{UL}}$ stands for the generated interference to the FS receive antenna k generated by the transmission from UE j to its associated BS i, and $P_{\text{UE},j}^{\text{Tx}}$ is transmit power at UE j. Note that the transmit power from UE is assumed to be controlled with an LTE-like uplink power control mechanism [34]. The uplink power control (TPC) at

the UE is assumed to be the same as the LTE system and as follows [34]:

$$P_{\text{UE},j}^{\text{Tx}} = P_{\max} \times \min\left\{1, \max\left[R_{\min}, \left(\frac{PL}{PL_{x-ile}}\right)^{\gamma}\right]\right\} \quad (9)$$

where $P_{\text{UE},j}^{\text{Tx}}$ is the transmit power at UE j, $P_{\max}$ is the maximum transmit power, $R_{\min}$ is the ratio of UE minimum and maximum transmit powers, i.e., $P_{\min}/P_{\max}$ and determines the minimum power reduction ratio to prevent UEs with good channel conditions to transmit at very low power level, i.e., it is $-64\,\text{dB}$ if the UE's maximum and minimum transmit powers are 24 dBm and $-40\,\text{dBm}$, PL is the path-loss for the UE from its serving BS, PL_{x-ile} is an x-percentile path-loss (plus shadowing) value. Finally, $0 < \gamma \le 1$ is the balancing factor for UEs with bad channel and UEs with good channel conditions. In addition, $L\left(f_c, d_{(j,k)}\right)$ and $G_{\text{FS},k}^{\text{Rx}}(\varphi^*, \theta^*)$ are as defined in Section IV-B.1; and corresponding angular illustrations are in Fig. 8. Lastly, the effect from the bandwidth difference between FS and UE should be taken account as well with (5).
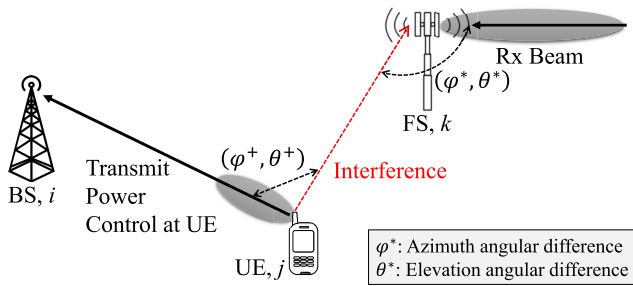

FIGURE 8. Illustration of uplink interference scenarios.

After calculating individual uplink interference with (8), overall accumulated interference (i.e., $\mathcal{I}$ in (2)) at an FS receiver antenna can be obtained by summing all calculated uplink interference values in a linear scale as follows:

$$\mathcal{I} = \sum_{\forall i \in S_{\text{BS}}} \sum_{\forall j \in S_{\text{UE},i}} I_{(i,j)}^{\text{UL}} \quad (10)$$

where S_{BS} is a set of micro-cellular BSs and $S_{\text{UE},i}$ is a set of the UEs that is associated with micro-cellular BS $i \in S_{\text{BS}}$.

C. ADJACENT-CHANNEL INTERFERENCE CALCULATION
Not only co-channel interference components which can be calculated as explained in Section IV-B, interference due to adjacent channel sensitivity can be also taken account due to the fact that the channel bandwidth of BS/UE is much larger than the channel bandwidth of FS. In this work, 40 dB, 50 dB, and 60 dB less interferences are assumed compared to the co-channel interference component in the first, second, and third adjacent channel interference, respectively.

The final $\mathcal{I}^*$ in (2) can be calculated by the summation of co-channel interference $\mathcal{I}$ ((7) for downlink interference and (10) for uplink interference) and adjacent channel interference.
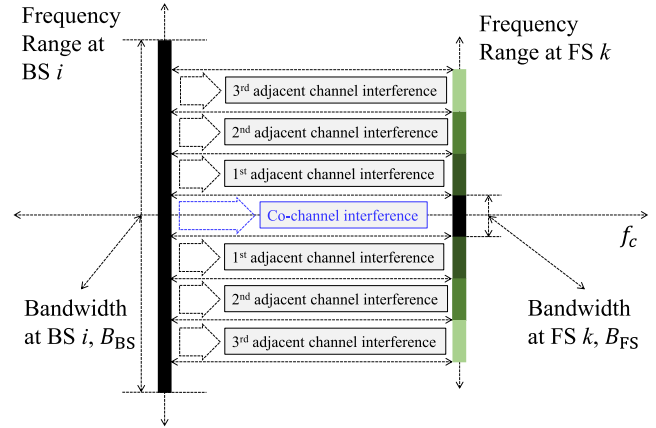

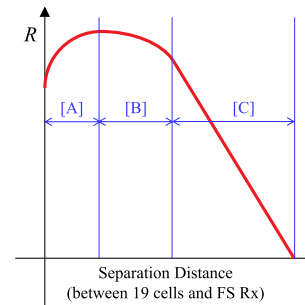**FIGURE 9.** Illustration for the 1st, 2nd, and 3rd adjacent channel interference components.

FIGURE 10. Illustration for graph interpretation.
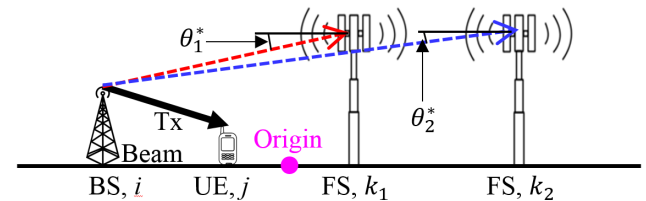

FIGURE 11. Illustration for graph interpretation in the [A] and [B] in Fig. 10. Note that the *origin* in this figure means the point where the separation distance is 0 Km (refer to Section II).

V. FREQUENCY SHARING STUDY RESULTS IN MILLIMETER-WAVE BANDS
A. GRAPH INTERPRETATION
The simulation results will be plotted as illustrated in Fig. 10. In Fig. 10, x-axis stands for the distance between 19 small cells and FS receiver; and y-axis stands for the required frequency rejection R and this R can be calculated using (2). If $R > 0$ in Fig. 10, we need to suppress R amount of interference, and investigate any kinds of interference mitigation schemes for the operation of the FS receiver antenna. On the other hand, we do not need to suppress interference, and thus we do not need to consider interference mitigation schemes when $R \le 0$ 10.

The plotting results in Fig. 10 show three different behaviors depending on the separation distance, i.e., the regions [A], [B], and [C]. In order to explain the behaviors, we have an example illustration as shown in Fig. 11. In Fig. 11,
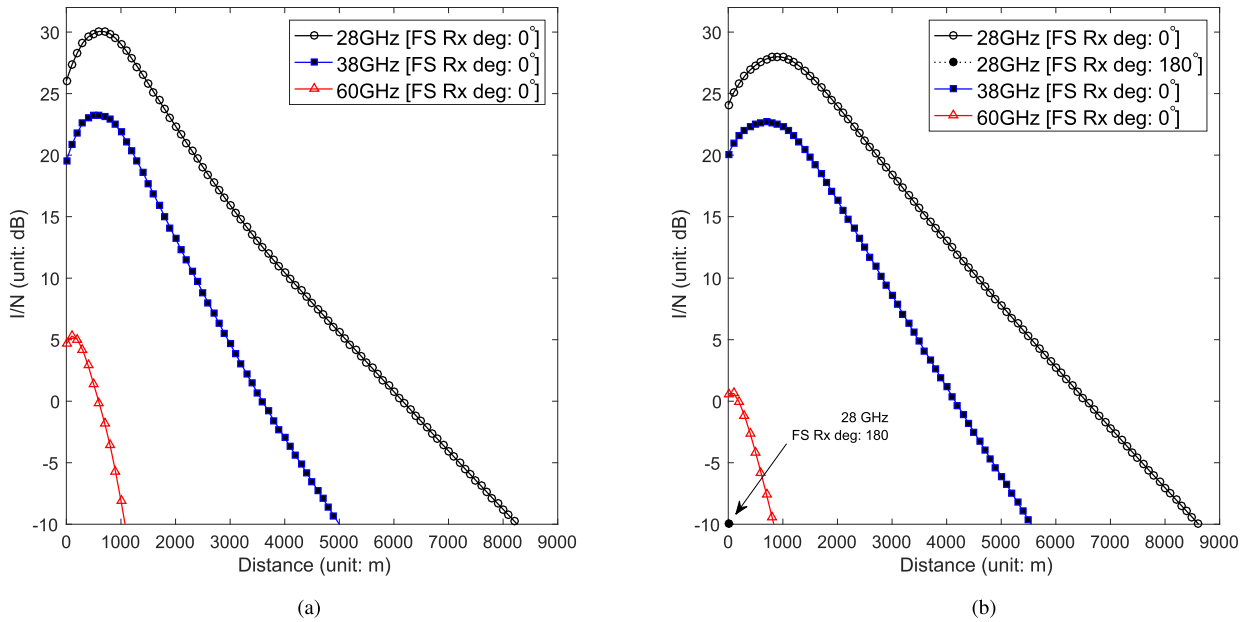
FIGURE 12. Frequency sharing study for downlink and uplink interference scenarios in 28 GHz, 38 GHz, and 60 GHz bands. (a) Donwlink. (b) Uplink.

two R values are compared when FS Rx antennas are at k_1 or k_2. Note the distance between origin and k_1 is small in [A]; the distance between origin and k_2 is also small; and we suppose that k_1 is closer to the origin than k_2. In this case, we can define θ_1^* and θ_2^* as shown in Fig. 11 and explained in Section IV-B, Fig. 6, and Fig. 8. Then, it is obvious that $G_{FS,k}^{Rx}\left(\varphi_1^*, \theta_1^*\right) < G_{FS,k}^{Rx}\left(\varphi_2^*, \theta_2^*\right)$ when k_2 is farther from origin than k_1. In addition, $L\left(f_c, d_{(i,k)}\right)$ (in (6), i.e., path-loss including oxygen/rain attenuations) is not yet dominant if the distance between BS i and FS Rx is small. That's why if the FS receiver station becomes farther from origin within region [A], the R increases. In the region [B] of Fig. 10, the impacts of $L\left(f_c, d_{(i,k)}\right)$ (in (6) increases while the separation distance becomes longer. In addition, the angular difference between θ_1^* and θ_2^* becomes smaller. Therefore, the R starts to decrease. In the region [C] of Fig. 10, the R linearly decreases in a dB scale because the impacts from $L\left(f_c, d_{(i,k)}\right)$ become much larger than the impacts in [B] (note that $L\left(f_c, d_{(i,k)}\right)$ is a linear function of $d_{(i,k)}$ in a dB scale).

B. SIMULATION RESULTS

The required frequency rejection in downlink and uplink interference scenarios are simulated and the results are presented in Fig. 12(a) and 12(b), respectively. We performed Monte Carlo simulations with 100 iterations due to the randomness of UE positions in each sector. In Fig. 12(a) and Fig. 12(b), x-axis and y-axis represent the separation distance from the origin (refer to Fig. 1) up to 10 Km and the required frequency rejection (R, calculated by (2)), respectively.

If the antenna orientation of an FS receive station is 180° in Fig. 1, R is not positive in both downlink and uplink interference scenarios in 38 GHz and 60 GHz bands. This means that

TABLE 4. Threshold distances for the case where $R > 0$ in (2).

	28 GHz	38 GHz	60 GHz
Downlink situations	8.2 Km	4.9 Km	1.0 Km
Uplink situations	8.6 Km	5.5 Km	0.8 Km

we do not need to mitigate interference for the protection of the operation of FS. In addition, R is not positive in downlink interference scenario in 28 GHz when the antenna orientation of an FS receive station is 180° in Fig. 1, i.e., interference mitigation is not required. If the antenna orientation of an FS receive station is 180° in uplink interference scenario, interference mitigation is required only when the distance between 19 small cells and FS receive station is very small, i.e., less than 100 m ($R \approx 0.0844$ dB), as presented in Fig. 12(b).

In downlink interference scenario, we need to suppress certain amounts of interference as plotted in Fig. 12(a). Up to certain distances in various situations (for both downlink and uplink scenarios, and for each carrier frequency), we need to suppress interference and the y-axis in the figure shows the amounts of interferences which should be suppressed. The distance values those are minimum distances which are for safe co-existence between FS systems and small cell systems are summarized in Table 4.

Note that we only consider the ITU Region Q with 1% outage to observe the worst case performance in terms of rain attenuation factors. In addition, various rain impacts in 60 GHz can be observed in [2].

C. SUMMARY

As shown in Fig. 12, the R curve in 60 GHz shows the very low interference levels and the dropping rate is very dramatic

because of the high attenuation in 60 GHz including path-loss, oxygen attenuation, and rain attenuation. In addition, the *R* curve in 28 GHz shows the highest interference level among the considering three bands because of (i) low attenuation factors (including path-loss, oxygen attenuation, and rain attenuation) and (ii) the narrowest channel bandwidth.

Therefore, these results show that 60 GHz mmWave technology is the best option in terms of co-existence with FS systems and we do not need to implement high-performance and high-cost interference mitigation schemes for the technology. Essentially, this is because of high attenuation factors in path-loss. On the other hand, we need to implement any interference mitigation schemes if we want to use 28 GHz and 38 GHz wireless technologies for cellular networks.

If our cellular deployment targets longer distances than the maximum distance of 60 GHz mmWave systems under certain data rate requirements, the other 28 GHz or 38 GHz carrier frequencies should be considered for the requirements.

VI. 60 GHz INTEGRATED MAA PLATFORM

Traditional antenna system architectures are generally not capable of combining wide-angles with high directionality. To achieve the necessary wide directionality, the phased antenna arrays should consist of a large number of antenna elements [35], [36]. Nowadays, the phased antenna array architectures are widely used for mass production and intended for personal mobile devices comprise of a single module containing an RF integrated circuits (RFIC) chip that includes controlled analogue phase shifters capable of providing several phase shifting levels. The antenna elements are connected to the RFIC via feeding lines. According to the loss on the feeding lines, this approach allows implementing antenna arrays with limited dimensions of up to 8-by-8 thus achieving gains of about 15-20 dB as observed in our measurements.
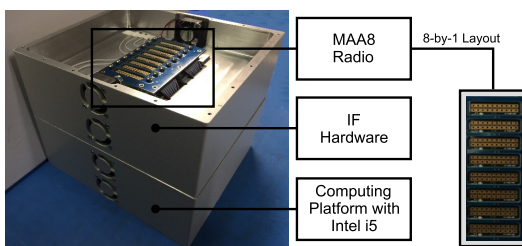

FIGURE 13. Integrated 60 GHz mmWave MAA architectures and snapshots. The MAA box consists of three major components, including MAA8 radio (i.e., modular antenna array with 8 modules), IF hardware (i.e., intermediate frequency hardware), and computing platform with Intel i5 CPU.

One of novel antenna array architectures for the 60 GHz band that provides simultaneous flexibility in form factor choice, beam steering, and high array gain in a conceivably more cost-efficient manner is to construct modular antenna arrays. Each module is implemented in a traditional way with dedicated RFIC serving several antenna elements and an RF beamforming unit. This MAA RF architecture is as illustrated in Fig. 13 and its high level block diagram is
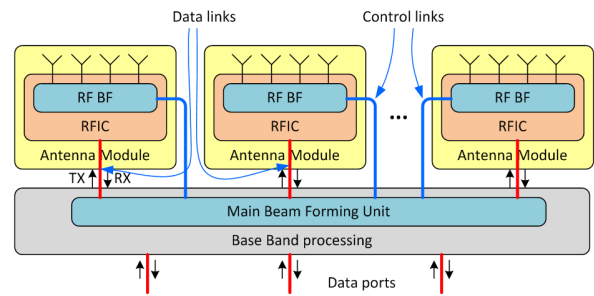

FIGURE 14. High-level block diagram of the Intel MAA architecture.

illustrated in Fig. 14. Traditional antenna architectures used in mmWave band are, generally, not capable of combining wide angle coverage with high directivity. Existing reflective, parabolic dishes and lens antennas can create narrow beam, thus delivering the needed 30-40 dB antenna gain [24], but they lack the flexibility to cover wide angle coverage and are relatively bulky. Phased patch antenna arrays allows steering the beam to a desired direction. However, to achieve the necessary directivity, the array must consist of a large number of elements (several hundred to thousands). Antenna array architectures currently used for mass production and intended for personal devices employ a single module, containing an RFIC chip that includes controlled analogue phase shifters capable of providing several discrete phase shifting levels. The antenna elements are connected to the RFIC chip via feed lines. However, due to the loss inherent in the feed lines, this approach reduces antenna gain and efficiency, and becomes a severe problem when the number of antenna elements and RF increase [37]–[39]. To overcome this limitation, we propose an MAA architecture that provides flexibility in form factor choice, beam steering, and array gain in a cost effective manner. The architecture is shown in Fig. 14 and is essentially a type of massive multiple-input multiple-output (MIMO) system. However, instead of using an individual antenna module, MAA is constructed using modular, composite mmWave antenna arrays. Each module is implemented with a dedicated RFIC chip serving several antenna elements and an RF beamforming (RF-BF) unit with discrete phase shifters. Note that the size of one element in MAA is approximately 5 mm-by-5 mm. Given its modularity, the length of the feed lines in the MAA architecture can be kept much shorter hence incurring much lower feed line loss. This makes the MAA architecture much more flexible and efficient than existing approaches.

The aperture of MAA and total transmitted power may exceed that of an individual sub-array module proportionally to the number of the sub-array modules used in a linear scale. Therefore, much narrower beams may be created and, thus, much greater antenna gains may be achieved with the MAA rather than individual sub-arrays. It is also possible that sectors of different sub-arrays may be configured in such a way as to vary the coverage angle of the composite array, thereby creating several coverage angles. Each sub-array module has
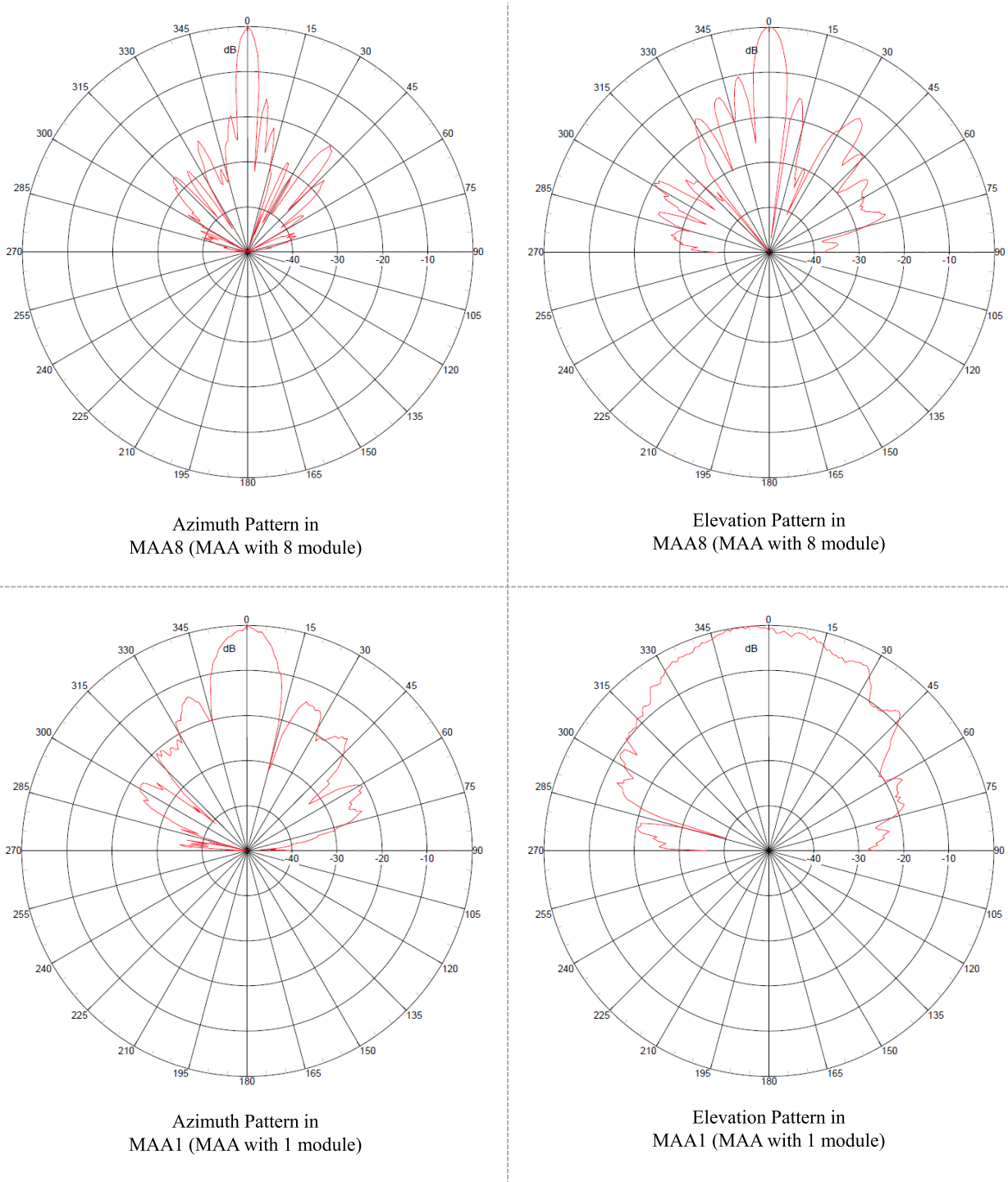
Azimuth Pattern in
MAA8 (MAA with 8 module)

Elevation Pattern in
MAA8 (MAA with 8 module)

Azimuth Pattern in
MAA1 (MAA with 1 module)

Elevation Pattern in
MAA1 (MAA with 1 module)

FIGURE 15. **Existing measured MAA radiation patterns (MAA8 is for BS and MAA1 is for UE).**

an 8-by-2 elements where the transmit power and the transmit antenna gain of one MAA are determined as 10 dBm and 15 dBi. Note that these are measured values. In Fig. 13, currently developing integrated 8-module MAA prototype is presented. More details about this MAA architecture is presented in [40].

VII. FREQUENCY SHARING STUDY RESULTS WITH PRACTICAL 60 GHz MAA RADIATION PATTERNS

The theoretical simulation research results in Section V is based on ITU-R F.1336 standardized radiation patterns. However, the practical MAA based simulation study is additionally performed in this section. The antenna radiation

patterns in azimuth and elevation planes are measured as shown in Fig. 15 based on MAA modules.
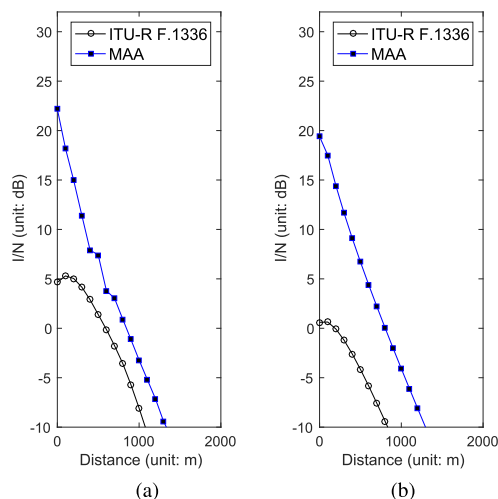

FIGURE 16. *R* comparison between ITU-R F.1336 and measured MAA patterns in 60 GHz bands. For this simulation study, MAA8 (MAA with 8 modules) is used for FS and BS, and MAA1 (MAA with 1 module) is used for UE. (a) Downlink. (b) Uplink.

As presented in Fig. 16(a) and Fig. 16(b), the required frequency rejection *R* with existing MAA is higher than the *R* with ITU-R F.1336 standardized patterns because of following two reasons: (i) the measured elevation patterns are much larger than the patterns with ITU-R F.1336 as shown in Fig. 15 and Fig. 2; and (ii) the measured azimuth patterns have high sidelobe levels as shown in Fig. 15.

The gap between the *R* in measured patterns and the *R* in ITU-R F.1336 is larger in uplink interference scenarios as shown in Fig. 16(b) due to the fact that the pattern difference between MAA and ITU-R F.1336 is the largest in the elevation plane of MAA1 (UE antenna radiation pattern).

VIII. CONCLUDING REMARKS AND FUTURE RESEARCH DIRECTIONS

This paper presents 28 GHz, 38 GHz, and 60 GHz millimeter-wave (mmWave) sharing study results between small cells and fixed service (FS) stations in terms of required frequency rejection depending on various separation distance and the antenna directions of an FS receive station (0° and 180°). In this frequency sharing study, we calculate the amount of downlink and uplink interferences accumulated in an FS receive antenna; and then we determine how much interference should be suppressed/mitigated to prevent from harmful interference. This research is essential and mandatory for deploying mmWave cellular systems in order to verify whether the deploying systems inject harmful interference to existing fixed service (FS) systems or not. If the deploying systems generate the interference, additional interference mitigation schemes should be introduced. Therefore, this type of research is required in order to introduce new frequency bands in currently existing networks. As a result, we numerically verify how much interference should be suppressed.

In downlink interference, no interference mitigation schemes are required if FS antenna faces opposite to cellular networks. If the FS antenna faces cellular networks directly, 28 GHz, 38 GHz, and 60 GHz bands systems should be separated from FS systems at least 8.2 Km, 4.9 Km. and 1.0 Km, respectively. In uplink interference, no interference mitigation schemes are required if FS antenna faces opposite to the cells in 38 GHz and 60 GHz bands. In 28 GHz, 100 m separation distance between FS systems and cellular systems for co-existence. If FS antenna faces the cells directly in uplink interference, 28 GHz, 38 GHz, and 60 GHz bands systems should be separated from FS systems at least 8.6 Km, 5.5 Km. and 0.8 Km, respectively.

In addition, one potential interference mitigation scheme is introduced and the performance with the existence of the interference mitigation scheme is also evaluated. The result says that approximately 4.1 dB reduction can be achieved even if simple interference mitigation schemes are utilized.

Lastly, additional frequency sharing study is performed with existing measured modular antenna array (MAA) radiation patterns instead of theoretical standardized patterns. The MAA RF systems/hardware has been well studied due to its flexibility and efficiency. We have been working for the MAA in order to use the solution for 60 GHz IEEE 802.11ad products. The sharing study results with existing mmWave MAA is worse (i.e., injecting more harmful interference to FS systems) than the study with ITU-standard radiation patterns because of following reasons: (i) MAA RF solution contains certain amounts of sidelobes and (ii) larger elevation half power-beamwidth (HPBW) than theoretical HPBW. This performance gap should be reduced when next-generation MAA solutions have better radiation patterns.

As future research directions, following topics are of our interests. First, we will conduct similar frequency sharing study for other potential frequency bands including E-bands. Furthermore, another antenna solutions are of our interests because they also provides another types of antenna radiation patterns. Lastly, our MAA solutions evolves and its antenna radiation patterns are getting better in terms of sidelobe reduction. Therefore, we will keep continue frequency sharing study with upcoming MAA solutions.

REFERENCES

[1] J. Kim, L. Xian, R. Arefi, A. Maltsev, and A. S. Sadri, "Study of coexistence between 5G small-cell systems and systems of the fixed service at 39 GHz band," in *IEEE MTT-S Int. Microw. Symp. Dig.*, May 2015, pp. 1–3.

[2] J. Kim, L. Xian, R. Arefi, and A. S. Sadri, "60 GHz frequency sharing study between fixed service systems and small-cell systems with modular antenna arrays," in *Proc. IEEE GLOBECOM Workshop*, Dec. 2015, pp. 1–6.

[3] T. S. Rappaport *et al.*, "Millimeter wave mobile communications for 5G cellular: It will work!" *IEEE Access*, vol. 1, pp. 335–349, 2013.

[4] Y. Azar *et al.*, "28 GHz propagation measurements for outdoor cellular communications using steerable beam antennas in New York City," in *Proc. IEEE Int. Conf. Commun. (ICC)*, Jun. 2013, pp. 5143–5147.

[5] H. Zhao *et al.*, "28 GHz millimeter wave cellular communication measurements for reflection and penetration loss in and around buildings in New York City," in *Proc. IEEE Int. Conf. Commun. (ICC)*, Jun. 2013, pp. 5163–5167.

[6] M. Samimi *et al.*, "28 GHz angle of arrival and angle of departure analysis for outdoor cellular communications using steerable beam antennas in New York City," in *Proc. IEEE Veh. Technol. Conf. (VTC Spring)*, Jun. 2013, pp. 1–6.

[7] W. Roh *et al.*, "Millimeter-wave beamforming as an enabling technology for 5G cellular communications: Theoretical feasibility and prototype results," *IEEE Commun. Mag.*, vol. 52, no. 2, pp. 106–113, Feb. 2014.

[8] W. Hong, K.-H. Baek, Y. Lee, Y. Kim, and S.-T. Ko, "Study and prototyping of practically large-scale mmWave antenna systems for 5G cellular devices," *IEEE Commun. Mag.*, vol. 52, no. 9, pp. 63–69, Sep. 2014.

[9] T. S. Rappaport, F. Gutierrez, Jr., E. Ben-Dor, J. N. Murdock, Y. Qiao, and J. I. Tamir, "Broadband millimeter-wave propagation measurements and models using adaptive-beam antennas for outdoor urban cellular communications," *IEEE Trans. Antennas Propag.*, vol. 61, no. 4, pp. 1850–1859, Apr. 2013.

[10] J. Kim and E.-S. Ryu, "Quality of video streaming in 38 GHz millimetre-wave heterogeneous cellular networks," *Electron. Lett.*, vol. 50, no. 21, pp. 1526–1528, Oct. 2014.

[11] J. M. Gilbert, C. H. Doan, S. Emami, and C. B. Shung, "A 4-Gbps uncompressed wireless HD A/V transceiver chipset," *IEEE Micro*, vol. 28, no. 2, pp. 56–64, Mar. 2008.

[12] T. S. Rappaport, J. N. Murdock, and F. Gutierrez, Jr., "State of the art in 60-GHz integrated circuits and systems for wireless communications," *Proc. IEEE*, vol. 99, no. 8, pp. 1390–1436, Aug. 2011.

[13] S. Wyne, K. Haneda, S. Ranvier, F. Tufvesson, and A. F. Molisch, "Beamforming effects on measured mmWave channel characteristics," *IEEE Trans. Wireless Commun.*, vol. 10, no. 11, pp. 3553–3559, Nov. 2011.

[14] J. Park, S. L. Kim, and J. Zander, "Tractable resource management with uplink decoupled millimeter-wave overlay in ultra-dense cellular networks," *IEEE Trans. Wireless Commun.*, vol. 15, no. 6, pp. 4362–4379, Jun. 2016.

[15] B. Ma, H. Shah-Mansouri, and V. W. S. Wong, "Multimedia content delivery in millimeter wave home networks," *IEEE Trans. Wireless Commun.*, vol. 15, no. 7, pp. 4826–4838, Jul. 2016.

[16] G. Lee, Y. Sung, and J. Seo, "Randomly-directional beamforming in millimeter-wave multiuser MISO downlink," *IEEE Trans. Wireless Commun.*, vol. 15, no. 2, pp. 1086–1100, Feb. 2016.

[17] T. S. Rappaport, G. R. Maccartney, M. K. Samimi, and S. Sun, "Wideband millimeter-wave propagation measurements and channel models for future wireless communication system design," *IEEE Trans. Commun.*, vol. 63, no. 9, pp. 3029–3056, Sep. 2015.

[18] M. Peter, R. J. Weiler, T. Kuhne, B. Goktepe, J. Serafimoska, and W. Keusgen, "Millimeter-wave small-cell backhaul measurements and considerations on street-level deployment," in *Proc. IEEE GLOBECOM Workshops (GC Wkshps)*, Dec. 2015, pp. 1–6.

[19] K. Haneda, "Channel models and beamforming at millimeter-wave frequency bands," *IEICE Trans. Commun.*, vol. E98-B, no. 5, pp. 755–772, May 2015.

[20] M. Kyrö, S. Ranvier, V. M. Kolmonen, K. Haneda, and P. Vainikainen, "Long range wideband channel measurements at 81–86 GHz frequency range," in *Proc. 4th Eur. Conf. Antennas Propag. (EuCAP)*, Apr. 2010, pp. 1–5.

[21] G. R. Maccartney, T. S. Rappaport, M. K. Samimi, and S. Sun, "Millimeter-wave omnidirectional path loss data for small cell 5G channel modeling," *IEEE Access*, vol. 3, pp. 1573–1580, Sep. 2015.

[22] *System Parameters and Considerations in the Development of Criteria for Sharing or Compatibility Between Digital Fixed Wireless Systems in the Fixed Service and Systems in Other Services and Other Sources of Interference*, Rec. ITU-R F.758-5, ITU Recommendation, Mar. 2012.

[23] J. Kim and A. F. Molisch, "Quality-aware millimeter-wave device-to-device multi-hop routing for 5G cellular networks," in *Proc. IEEE Int. Conf. Commun. (ICC)*, Jun. 2014, pp. 5251–5256.

[24] J. Kim, Y. Tian, S. Mangold, and A. F. Molisch, "Joint scalable coding and routing for 60 GHz real-time live HD video streaming applications," *IEEE Trans. Broadcast.*, vol. 59, no. 3, pp. 500–512, Sep. 2013.

[25] *Reference Radiation Patterns of Omnidirectional, Sectoral and Other Antennas for the Fixed and Mobile Service for Use in Sharing Studies in the Frequency Range From 400 MHz to About 70 GHz*, Rec. ITU-R F.1336-4, ITU Recommendation, Feb. 2014.

[26] *Propagation Data and Prediction Methods for the Planning of Short-Range Outdoor Radiocommunication Systems and Radio Local Area Networks in the Frequency Range 300 MHz to 100 GHz*, Rec. ITU-R P.1411-8, ITU Recommendation, Jul. 2015.

[27] *Attenuation by Atmospheric Gases*, Rec. ITU-R P.676-10, ITU Recommendation, Sep. 2013.

[28] FCC, "Millimeter Wave Propagation: Spectrum Management Implications," Bulletin No. 70, Jul. 1997.

[29] *Characteristics of Precipitation for Propagation Modelling*, Rec. ITU-R PN.837-1, ITU Recommendation, 1994.

[30] S. Singh, R. Mudumbai, and U. Madhow, "Interference analysis for highly directional 60-GHz mesh networks: The case for rethinking medium access control," *IEEE/ACM Trans. Netw.*, vol. 19, no. 5, pp. 1513–1527, Oct. 2011.

[31] "Possibility of sharing between fixed links and SNG in the 14.25-14.5 GHz band," in *Proc. Eur. Radiocommun. Committee Eur. Conf. Postal Telecomm. Admin.*, Oct. 1996.

[32] Millimetre-Wave Evolution for Backhaul and Access (MiWEBA), "WP4: Radio Resource Management for mm-wave Overlay HetNets," *EU Contract No. FP7-ICT-608637*, Dec. 2015.

[33] *Calculation of Free-Space Attenuation*, Rec. ITU-R P.525-2, ITU Recommendation, Aug. 1994.

[34] *Evolved Universal Terrestrial Radio Access (E-UTRA); Radio Frequency (RF) System Scenarios*, document 3GPP 36.942, 3GPP, 2012.

[35] S. Ramesh and T. Rao, "Indoor radio link characterization studies for millimeter wave wireless communications utilizing dielectric-loaded exponentially tapered slot antenna," *J. Electromagn. Waves Appl.*, vol. 29, no. 4, pp. 551–564, 2015.

[36] P. Shrivastava and R. R. Thipparaju, "60 GHz radio link characteristic studies in hallway environment using antipodal linear tapered slot antenna," *IET Microw., Antennas Propagat.*, vol. 9, no. 15, pp. 1793–1802, 2015.

[37] U. Johannsen, M. I. Kazim, A. B. Smolders, and M. Herben, "Modular antenna array concept for millimeter-wave beam-steering applications," in *Proc. Prog. Electromagn. Res. Symp.*, Aug. 2013, pp. 229–234.

[38] S. S. Holland and M. N. Vouvakis, "The planar ultrawideband modular antenna (PUMA) array," *IEEE Trans. Antennas Propag.*, vol. 60, no. 1, pp. 130–140, Jan. 2012.

[39] A. Garrod, "Digital modules for phased array radar," in *Proc. IEEE Int. Phased Array Syst. Technol. Symp.*, May 1995, pp. 726–731.

[40] R. J. Weiler *et al.*, "Enabling 5G backhaul and access with millimeter-waves," in *Proc. Eur. Conf. Netw. Commun. (EuCNC)*, Jun. 2014, pp. 1–5.

JOONGHEON KIM received the B.S. and M.S. degrees in Computer Science from Korea University, Seoul, South Korea, in 2004 and 2006, respectively, and the Ph.D. degree from the University of Southern California (USC), USA, in 2014. Before joining USC, he was a Research Engineer with LG Electronics, Seoul, from 2006 to 2009. From 2013 to 2016, he was a Systems Engineer with Intel Corporation, Santa Clara, CA, USA, where he was involved in mmWave Standards and Advanced Technology Team for 60 GHz modular antenna array platforms and standardization contributions. Since 2016, he has been an Assistant Professor with Chung-Ang University, Seoul. His current research interests include mmWave backhaul/access radio platforms. He is an author of more than 50 international publications and also holds more than 20 granted international patents for mmWave video streaming and the IEEE 802.11ad/WiGig standards. He was awarded the Annenberg Graduate Fellowship with his Ph.D. admission from USC, in 2009.

LIANG XIAN received the Ph.D. degree in electrical engineering and computer science from Oregon State University, Corvallis, OR, USA. He was a Senior Wireless/DSP Engineer with Summit Semiconductor, Hillsboro, OR, USA, from 2010 to 2013 and also a Senior System Engineer with Focus Enhancements, Hillsboro, from 2006 to 2010. Since 2013, he has been a Senior Wireless Standards Engineer with Intel Corporation, Hillsboro. His current research interests include mmWave backhaul/access radio prototyping.

ALI S. SADRI received the Ph.D. degree from North Carolina State University, Raleigh, NC, USA. His professional work started with IBM and as a Visiting Professor with Duke University, Durham, NC, USA. In 2002, he was with Intel Corporation, Mobile Wireless Division, where he is currently leading the mmWave and Wireless Gigabit (WiGig) standardization and advanced technology activities. He is currently a Senior Director of the Intel Communications and Devices Group for mmWave Standards and Advanced Technology (mSAT) and the Chairman and CEO of the WiGig Alliance. He has over 20 years of engineering scientific and academic background. He holds over 25 issued patents in communications and wireless systems. His research interests include wireless communications theory, mmWave systems, channel modeling, adaptive closed loop power control, and adaptive modulations techniques.

Dr. Sadri has been presented in panel discussion and keynote presentation sessions for mmWave backhaul/access technologies at numerous major conferences, including the IEEE MTT-S International Microwave Symposium, the IEEE Custom Integrated Circuits Conference, the IEEE Global Communications Conference (GLOBECOM), and the IEEE International Conference on Communications.

· · ·